Controlling a Variable Stiffness Ankle Exoskeleton

Thesis by
Lorenzo Franceschini Shaikewitz

In Partial Fulfillment of the Requirements for the
Degree of
Minor in Controls and Dynamical Systems

Caltech

CALIFORNIA INSTITUTE OF TECHNOLOGY
Pasadena, California

2023
Defended June 1, 2023

Lorenzo Franceschini Shaikewitz
ORCID: 0009-0002-6698-3460

ACKNOWLEDGEMENTS

ABSTRACT

This decade has seen a proliferation in ankle exoskeletons designed for metabolic cost reduction. The most successful of these devices are cable-driven, requiring large torques and a rigid frame to achieve their goals. With recent advancements in compliant materials, it is now feasible to introduce a new class of lightweight, energy-reducing devices. We designed an ankle exoskeleton driven by handed shearing auxetics, one such compliant geometry that converts rotary actuation into linear displacement with variable stiffness. Simple control of this material coupled with our front-leg ankle exoskeleton design provides significant dorsiflexion assistance during normal walking under relatively low torques. We evaluated the device with one non-disabled subject on level ground. We present two designs that use this materials: one driven by brushless drone motors, and another driven by a powerful worm gearbox. We evaluate the former using electromyography and metabolic cost of transport. With one non-disabled subject on level ground, electromyography data clearly shows a significant reduction in soleus activity from use of the device. These results, however, do not translate into metabolic cost of transport. Use of the device increased the metabolic cost of transport by 5%. Although it did not achieve an energy reduction, these results demonstrate the potential of a lightweight soft ankle exoskeleton that better integrates with the human body.

TABLE OF CONTENTS

LIST OF ILLUSTRATIONS

Chapter 1

INTRODUCTION

Powered robotic exoskeletons have enormous potential to enhance human capabilities. Among the range of human functions, improving locomotion is of particular interest because of its ubiquity and importance in daily life. The average adult spends nearly 90 minutes of each day walking (Johansson et al., 2019). For some, locomotion and heavy lifting is an essential part of their occupation. Others who struggle with normal walking face many barriers navigating our world. Devices that reduce the energy cost of walking could make strenuous occupations easier and increase the quality of life for those who struggle with locomotion.

Ankle exoskeletons are a class of lower-limb exoskeletons that provide assistive forces to the ankle joint. By exerting an additional torque about the ankle, these devices have been shown to reduce the metabolic expenditure of non-disabled individuals across a range of walking speeds (Zhang et al., 2017; Luke M Mooney, Rouse, and Hugh M Herr, 2014; Slade et al., 2022). Furthermore, this supplementary torque has been shown to have additional mechanical advantages for individuals with locomotive impairments, such as improved gait symmetry for persons post-stroke (Takahashi, Lewek, and Gregory S Sawicki, 2015).

1.1 Previous Ankle Exoskeletons

The last two decades of research have seen enormous improvements in exoskeleton design and capabilities. The first prominent class of ankle exoskeletons was powered by pneumatic actuators. Ferris et al., 2006 developed an ankle exoskeleton that aligned pneumatics with key muscles, reducing soleus electromyography (EMG) root-mean-square by 65% during level-ground walking. Pneumatic force was applied as a function of lower-limb EMG signals, a method known as proportional myoelectric control. This development inspired a wave of other pneumatic ankle exoskeletons that used different control methods including footswitch-based timing (S. Galle et al., 2013), EMG signals (Takahashi, Lewek, and Gregory S Sawicki, 2015), and optimization of metabolic cost (Samuel Galle et al., 2017).

Early pneumatic ankle exoskeletons established several key results on user adaptation to exoskeleton assistance. Kao, Lewis, and Ferris, 2010 showed that exoskeleton

assistance during walking can modify human gait kinematics, but humans tend to return to their original joint moments as they get comfortable with the exoskeleton. S. Galle et al., 2013 confirmed these results, showing how an adaptation period can improve metabolic reduction from 9% to 16% compared to walking with an unpowered device. This result was achieved with actuation at a fixed percentage of the user's gait, as determined by a footswitch; although this simple control achieved large muscle activity reduction, the adaptation period suggests its limitations. Under this control scheme, the exoskeleton forces its user to adapt to assistance, rather than providing optimal assistance that adapts to the user.

While useful in the laboratory, pneumatic ankle exoskeletons require large air compressors that make them impractical for daily use. Further, they need heavy, customized attachments to mount to the body. Luke M Mooney, Rouse, and Hugh M Herr, 2014 presented a viable alternative to pneumatics with their untethered strut-based ankle exoskeleton. It used large cable-driven moment arms to generate an ankle torque without attempting to directly imitate a muscle, achieving an 11% reduction in the metabolic cost of walking under loaded conditions (Luke M. Mooney and Hugh M. Herr, 2016). The exoskeleton specifically targeted plantar flexion, demonstrating that push-off assistance can reduce metabolic cost of walking even under loaded conditions.

The use of metabolics to evaluate the effectiveness of ankle exoskeletons has become the *de facto* standard (Samuel Galle et al., 2017), providing a single number that captures the total energy cost of motion with and without exoskeleton assistance. The key metric for exoskeleton success is reducing metabolic cost compared to unpowered or normal walking. While useful for non-disabled individuals, it is important to remember that this number does not capture the complex effects of using an ankle exoskeleton including adaptation time, gait kinematics, or walking speed.

In recent years, many other ankle exoskeletons have been developed with increasingly large metabolic cost reductions. One prominent design replaces the struts used by Luke M Mooney, Rouse, and Hugh M Herr, 2014 with cables directly connected to the back of the foot to target push-off (Zhang et al., 2017). Using a human-in-the-loop optimization technique paired with a parameterized control curve, this design has achieved metabolic cost reductions of 24%. The addition of data-driven methods brought these results out of the laboratory setting, achieving 17% energy reduction compared to normal shoes and a consistently faster walking speed (Slade

et al., 2022).

These designs generally offer large mechanical power, leaving it to a control system to determine how best to apply the substantial available ankle torque. However, this is not the only approach. Collins, Wiggin, and Gregory S. Sawicki, 2015 designed a completely passive ankle exoskeleton that takes advantage of observed Achilles tendon dynamics. It used a spring-clutch mechanism attached to the back of the leg to selectively apply assistive forces, reducing metabolic cost of transport by 7% without any external power input (Collins, Wiggin, and Gregory S. Sawicki, 2015). This highlights the interplay between design and control; powerful exoskeletons can create substantial improvement with large torques and careful control, but well-designed exoskeletons can reduce energy cost with fixed control and no applied torque.

These designs were a major breakthrough in ankle exoskeleton development, promising impressive assistance without the need for nearby machinery. However, their use is heavily limited. Slade et al.'s cable-driven exoskeleton is a large, heavy machine with fast-moving cables and spools that require heavily customized shoes to function (Slade et al., 2022). Further, it is not clear how to generalize cable-driven exoskeletons to provide assistance to those with injury, muscle weakness, or gait asymmetries. The Collins passive design is lightweight, but has no capacity to adjust its control to different gaits (Collins, Wiggin, and Gregory S. Sawicki, 2015). There is no intermediate, untethered ankle exoskeleton that combines the generalizability enabled by actuation with a lightweight and safe design.

Advancements in compact and flexible actuators enable a transition away from heavy, rigid exoskeletons without sacrificing actuation. We present an ankle exoskeleton that uses recently developed handed shearing axuetics to generate linear motion. These soft materials enable a lightweight, compliant design with inherent, controllable spring-like dynamics. Although the strength of actuation is limited by the current state of these materials, our results demonstrate that even weak soft actuators can provide meaningful assistance during walking.

Chapter 2

BACKGROUND ON HANDED SHEARING AUXETICS

2.1   Handed Shearing Auxetic Geometry

Handed shearing auxetics (HSAs), first presented in Lipton et al., 2018, are composed of a basic tessellating geometry that is asymmetrical (handed) and expands perpendicular to shear (shearing auxetic). Specifically, the HSA unit cell geometry (shown in Figure 2.1) expands either left or right upon application of shear force.

To take advantage of this property, the HSA unit cell is tessellated into a cylindrical shape (Lipton et al., 2018). Now, a torsional load along the cylindrical axis produces a local shear load on the HSA unit cell, causing it to expand or contract. In cylindrical form, the unit cell's handedness determines whether the geometry will expand or contract under positive load. This procedure of expansion and contract is called the *axuetic trajectory*.

The complex geometry of HSAs typically requires them to be 3D printed in a rigid plastic (Good et al., 2021). Although the material itself must be rigid, the geometry is inherently compliant in both the normal and axial directions. All HSAs used in this project were 3D printed with Carbon FPU50 in collaboration with the University of Washington.

2.2   Tunable Properties

Further analysis of the cylindrical HSA geometry reveals several useful properties that may be tuned with mechanical adjustments. Handed shearing auxetics have a spring constant that changes as a function of applied torsion along the auxetic trajectory. This property allows them to be modeled essentially as a nonlinear spring. To match this model, suppose one end of the HSA cylinder is fixed and a torque is applied to the other end, generating a uniform torsional load throughout. To standardize across HSAs, consider the spring constant as a function of the angle of rotation θ of the non-fixed end. With this model comes a minimum energy length and holding torque for each θ (Good et al., 2021). An additional property is blocked force: the force required to counteract HSA extension or contraction when a torsional load is applied (Good et al., 2021).

These properties can be modified using several design parameters including cell

Conventional Auxetic

Shear Auxetic

θ_0 θ_1 θ_{max} θ_2 θ_3

Handed Shear Auxetic

θ_1 θ_{max} θ_2 θ_2 θ_{max} θ_1

Handed from Alignment

θ_1 θ_{max} θ_2 θ_2 θ_{max} θ_1
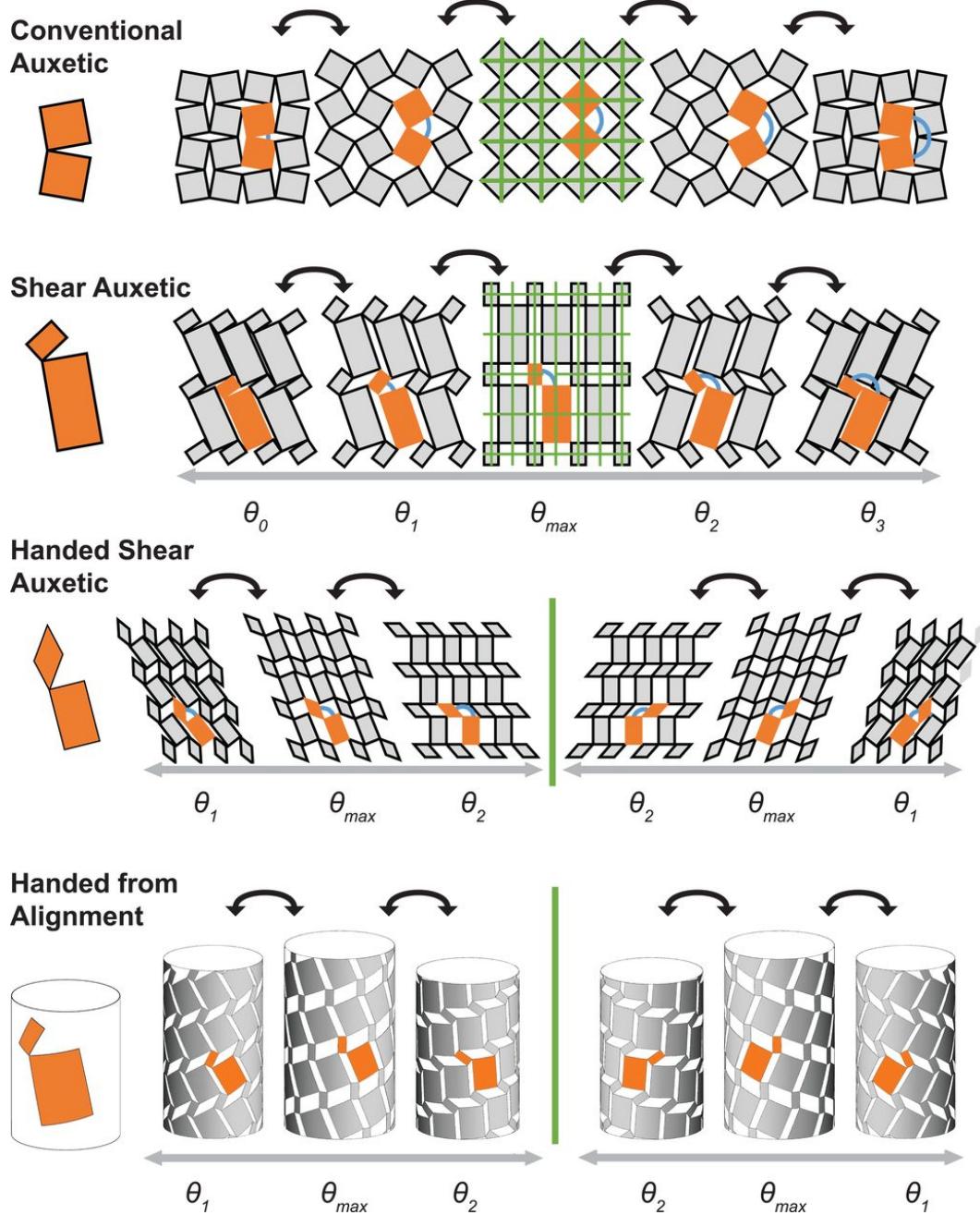
Figure 2.1: **HSA Unit Cell**. The basic geometric unit of the HSA is a handed shear auxetic tile. A conventional auxetic expands in all directions under load, but a shear auxetic expands primarily in the direction opposite to a shear load. Adding handedness causes the shear auxetic to twist either left or right under a shear load. Tiling this auxetic geometry into a cylinder produces a linear actuator that extends and contracts according to the applied torsion. This figure was first presented by Lipton et al., 2018.

size, base material, cylinder diameter, wall thickness, and row number. Previous work has studied the effect of these parameters on several performance metrics including resultant force, linear extension, and grip strength Truby, Chin, and Rus, 2021. These data allow selection of HSAs to match very specific design parameters, subject to inherent limitations of the material trajectory.

Another form of tuning is the printed position of the HSA cylinder along the auxetic trajectory (the "openness"), which corresponds to the zero-torque position of the HSA. Good et al., 2021 show how printed position influences the maximum compressive and tensional forces applied by the geometry. Specifically, "closed" HSAs (printed with the auxetic tilings unloaded) are capable of exerting forces in tension of at most 10 N, while "open" HSAs (printed with the auxetic tilings fully loaded) may exert large compressive forces but limited force in tension. Between these two extremes, an HSA may be printed in any degree of "openness" to trade off the desired compressive and tensional properties.

2.3 Soft Robotic Applications

Due to their handedness, multiple HSAs can form compact and compliant devices. For example, two opposite-handed HSAs fixed together at one end form a actuator that converts rotary motion (opposite torques on the HSAs) into linear actuation. The result is a zero-net-torque linear actuator that behaves like a nonlinear spring in the direction of actuation and can experience large deformations in the normal directions (Lipton et al., 2018). Other combinations of four or more HSAs can produce more complex actuators, but we primarily use the two-HSA linear form. This compact linear actuation is shown in Figure 2.2.

Recent works have successfully demonstrated this compliant method of actuation towards various soft robotic applications (Good et al., 2021; Truby, Chin, and Rus, 2021). However, it is important to note the significant limitations. HSAs printed with FPU50 are still relatively weak, capable of compressive forces of at most 10 N and tensional forces of at most 80 N (Good et al., 2021). Of course, these extremes are mutually exclusive: they depend on the printed auxetic position of the HSA. Large tensional forces also mean minimal length change and stiff behavior, while the compressive forces are less stiff but face smaller loads. This maximum force behavior significantly limits the capabilities of HSAs for robotic applications.

Our ankle exoskeleton demonstrates the application of HSAs towards compliant actuation of an ankle exoskeleton. Working within the broad design space of
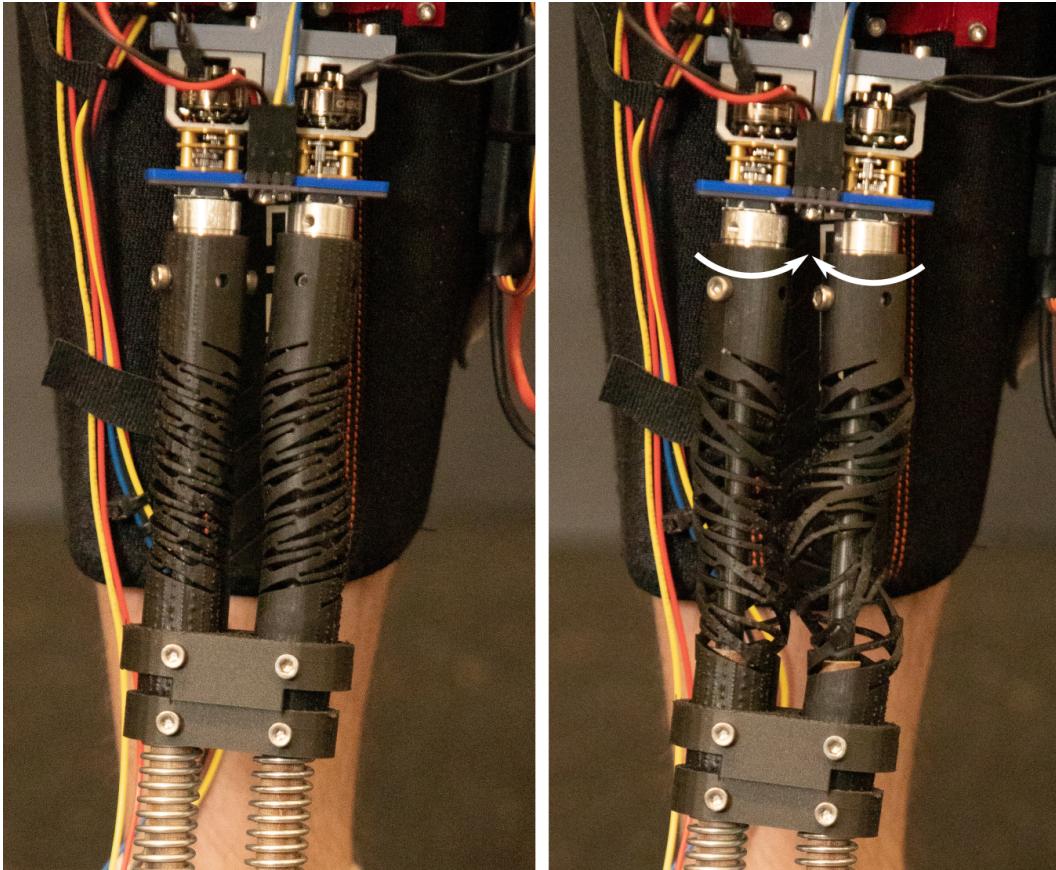
Figure 2.2: **HSA Mechanics**. A pair of left and right handed shearing auxetics (HSAs) generates linear motion when both are fixed at one end and opposite torsional loads are applied at the other end. We use rotary motors to drive this behavior, creating a complaint linear actuator.

HSAs, we customize both control parameters and HSA geometries to obtain optimal assistance for each individual.

Chapter 3

EXOSKELETON DESIGN

The ankle exoskeleton's design is driven by the use of HSA-based linear actuation to generate torques about the ankle. The design is divided into three subassemblies: shoe attachment (Section 3.2), shin attachment (Section 3.2), and the linear actuation stage between them (Section 3.2). Placement on the front of the leg braces the linear actuator on the shin and directs its forces onto the top of the foot. This positioning maximizes the moment that can be applied to the ankle during normal walking.

HSA compliance enables a lightweight and compact support structure, with the entire ankle exoskeleton weighing 490 grams/leg. Total torque is driven by choice of HSAs, which is discussed in Section 3.4. The full design is depicted in Figure 3.1.
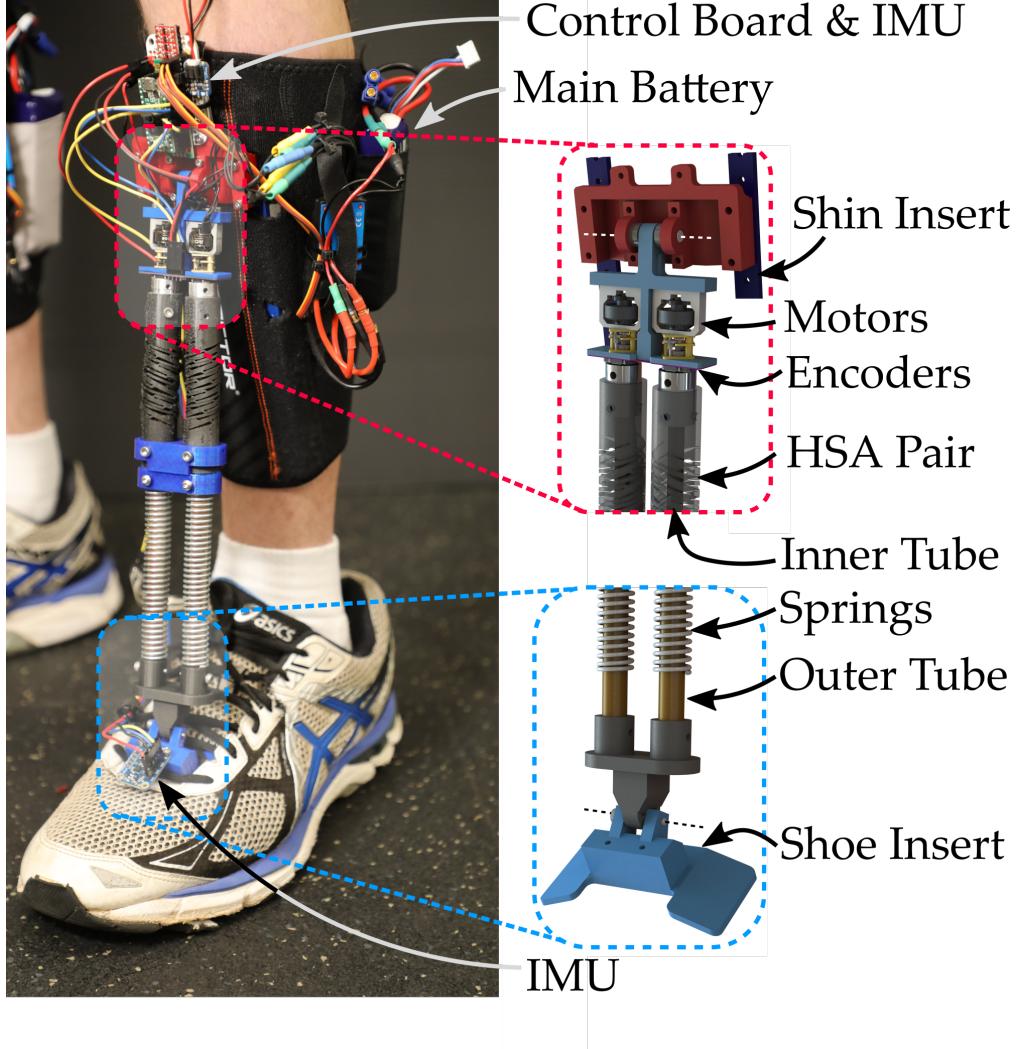
3.1 Motivation

With this device, we seek to introduce a new class of assistive ankle exoskeletons that are lightweight, highly customizable, and reduce the metabolic cost of normal walking. Reducing exoskeleton weight with more compliant actuators makes the devices easier to wear and more robust to unpredicted movements. Customizablity enables more effective control for individual users, and reducing the cost of walking for able-bodied individuals promises a broad range of benefits and an important step towards robotic devices for injury recovery.

Our use of HSAs meet these goals by enabling a compact linear actuator with a front-leg design and adjustable parameters. Paired with state estimation and control, we can achieve a metabolic reduction by targeting the push-off phase of the gait.
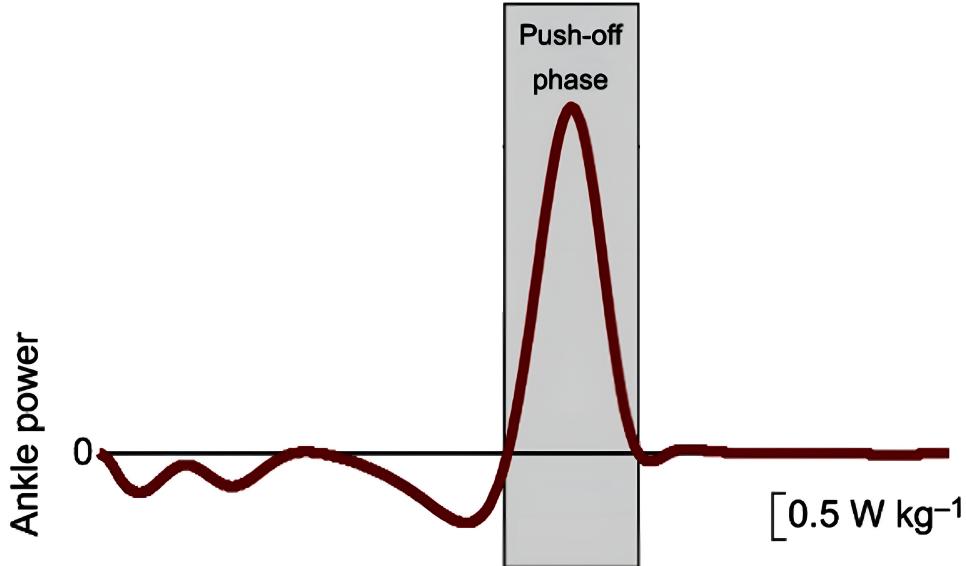
Gait Dynamics

To meet the goal of reducing metabolic cost effectively, the exoskeleton must apply appropriate torques when the body needs it. We identified two possible gait periods for metabolic improvement: (1) just before push-off, for healthy individuals and (2) towards the end of the swing phase, for those with drop-foot. Option (2) is particuarly promising for the weak HSA actuator, but was not explored further due to the risks of interacting with vulnerable individuals during the COVID-19 pandemic.

Figure 3.1: **Ankle Exoskeleton Design Detail.** Rotary motors actuate an HSA pair mounted on telescoping tubes to prevent buckling. Linear motion generated by the HSA pair changes the displacement position of a pair of springs mounted in series, modulating the force applied to the body. Shoe and shin inserts securely attach the device to the body and carry electronics.

Motivation for targeting the push-off period has precedent in gait moment analysis and exoskeleton design. From a gait moment perspective, Figure 3.2 shows qualitatively how ankle power peaks during the push-off period, providing an opportunity for assistance. Analysis by Zelik and Adamczyk, 2016 suggests that this large ankle moment is primarily caused by the elastic recoil of the Achilles tendon. Note that the steep drop-off in ankle power after the initial spike still occurs before the push-off phase is complete. This suggests that the body is particularly receptive to assistance

Figure 3.2: **Ankle Power During the Gait.** The ankle generates a significant amount of the propulsive force for walking during the push-off phase, when the Achilles tendon generates a large ankle moment (Zelik and Adamczyk, 2016). Note that this spike is power is temporary; there is a brief period immediately afterwards when push-off is still in progress but the body is incapable of applying additional ankle torque. This period is the primary target of our ankle exoskeleton. Note that this figure was modified from a version published by Zelik and Adamczyk, 2016.

during the end of the push-off phase, when the foot is still touching the ground but the recoil from the Achilles tendon is reduced.

This observation has been confirmed by a number of exoskeleton studies. Antonellis et al., 2022 use a hip exoskeleton to demonstrate that propulsion-targeted assistance provides superior performance. On the ankle exoskeleton side, the parameterized control curve used by Zhang et al., 2017 primarily targets push-off to achieve 24% metabolic reduction (see discussion in Section 1.1).

Motivation for Front-Leg Design

A front-leg design is somewhat unusual among the last decade of ankle exoskeletons. Our design departs from the norm to take advantage of unique actuator capabilities. We simultaneously demonstrate that front-leg mounting allows versatile and lightweight attachment to the body.

Many of the most successful ankle exoskeleton designs rely on actuation located behind the leg (Slade et al., 2022) or moment arms positioned on either side of

the leg (Luke M Mooney, Rouse, and Hugh M Herr, 2014) to produce a torque around the ankle. This paradigm traces back to a common feature among many previous exoskeleton designs: an operating mechanism that works better in tension than compression. The rope, in particular, is a feature of nearly every modern ankle exoskeleton design. In tension, it can transmit large forces to produce a desired moment, but in compression it lies in slack and does not transmit forces.

Rope-based designs are useful in part because of this variable stiffness property. The stiff tension behavior is conducive to transmitting forces, while the slack compressive behavior allows naturally efficient human dynamics to dominate at times when assistance is less efficient. However, the nature of this variable stiffness restricts its use in front-leg ankle exoskeletons. The control used by Slade et al., 2022; Luke M Mooney, Rouse, and Hugh M Herr, 2014 and others specifically targets push-off, when the plantarflexion angle increases rapidly. A front-leg design requires downward forces applied to the top of the foot, which is not directly achievable in tension.

The HSA-based linear actuator shares this variable-compliance property that makes rope so useful for ankle exoskeletons, but has a broader range of compliance behavior. A "closed" HSA may be designed to exert greater forces in compression than tension, allowing it to push off the top of the foot. In contrast, an "open" HSA generally exerts greater forces in tension, and a "half-open" HSA is capable of high stiffness in both modes. Informed HSA design, discussed in Section 3.4, enables an effective front-leg ankle exoskeleton. Additionally, some of the oldest pneumatics-based ankle exoskeleton designs use a front-leg mount, in part because pneumatics are able to exert forces in tension or compression (Ferris et al., 2006).

A key advantage of mounting acutation on the front of the leg is lightweight attachment. Rope-based designs that operate on the back on the leg require a heavily custom shoe (Luke M Mooney, Rouse, and Hugh M Herr, 2014) or significant shoe modification (Samuel Galle et al., 2017). A front-leg design allows for lightweight shoe inserts that are adjustable for any shoe size, as discussed in Section 3.2.

3.2 Mechanical Design Details

Shoe Attachment

The exoskeleton is mounted to the top of the foot via a 3D printed custom shoe insert, designed to fit at the base of the tongue of a typical laced shoe. It is secured to the shoe by shoelaces on top and pressure from the foot below. The bottom part

of the insert is padded to comfortably apply force to the top of the foot. The top part rises above the shoe, holding a lightly constrained revolute connection to the linear actuation stage and a 9-axis inertial measurement unit (IMU). This modular piece allows the user to use their own shoes for the exoskeleton. A single shoe insert may be used across different shoes and 2-3 US shoe sizes.

The shoe insert's revolute joint uses a pin connected through a larger hole to loosely constrain foot rotation. This leaves doris- and plantarflexion unconstrained while providing some compliance in the lateral and medial directions.

Linear Actuation Stage

The linear actuation stage between the foot and shin attachment points uses a pair of HSAs connected in series with parallel traditional springs (k_{eff} = 1.8 N/mm). The springs effectively override the dynamic spring constant of the HSAs, preserving the linear actuation property but insulating from stiffness changes. HSA motion is driven by a pair of rotary motors attached to the shin wrap. When these motors are driven in opposite directions, their torque causes the HSA assembly to extend or contract, changing the equilibrium position of the springs and pushing on the top of the foot. This creates a compliant system that can apply assistive force during push off without inhibiting the user's regular walking motion. To preserve HSA stiffness and prevent transverse bending, the linear actuation stage contains a complementary pair of telescoping tubes. Further detail on the motor configuration is described in Section 3.3.

Shin Attachment

A modified shin wrap secures the ankle exoskeleton to the anterior portion of the lower leg. This shin wrap is based on the Shock Doctor 857 Calf-Shin Wrap, which tightly attaches to the lower leg. We modified the padded vertical inserts on the 857 to provide a secure mounting location for one end of the linear actuation stage and key electronics. Unlike the joint on the shoe insert, the shin's connection to the linear actuator is a strict revolute joint. This freedom allows the user to change the angle between their foot and their leg but constrains lateral motion that may inhibit the exoskeleton's actuation.

For the drone motor variant of the design, the shin wrap also hosts the majority of the electronics needed to drive the device. A control board based on the Teensy 4.0 is mounted to the shin inserts just above the revolute joint. The control board also includes an IMU, electronic speed controllers, and 2.4 GHz two-way wireless

communication. Data from the IMUs at the shin and the foot separately undergo a standard Kalman filtering to estimate orientation. The exoskeleton transmits the relative quaternion, representing ankle angle, at a frequency of 100 Hz. A wire connecting to the shoe insert is required for this estimate. Power for this control board is provided by a small 1S lithium-polymer battery mounted between the board and the shin wrap.

Supporting electronics for control are connected to the shin control board. These include a force-sensative resistor (FSR) located below the heel, a load cell inline with the HSA stage, and motor potentiometers. Motor power is provided by a 3S lithium-polymer battery held in a pouch sewn onto the body of the shin wrap. Note that the worm gearbox variant of the design locates battery and electronics at the hip, as discussed in Section 3.2.
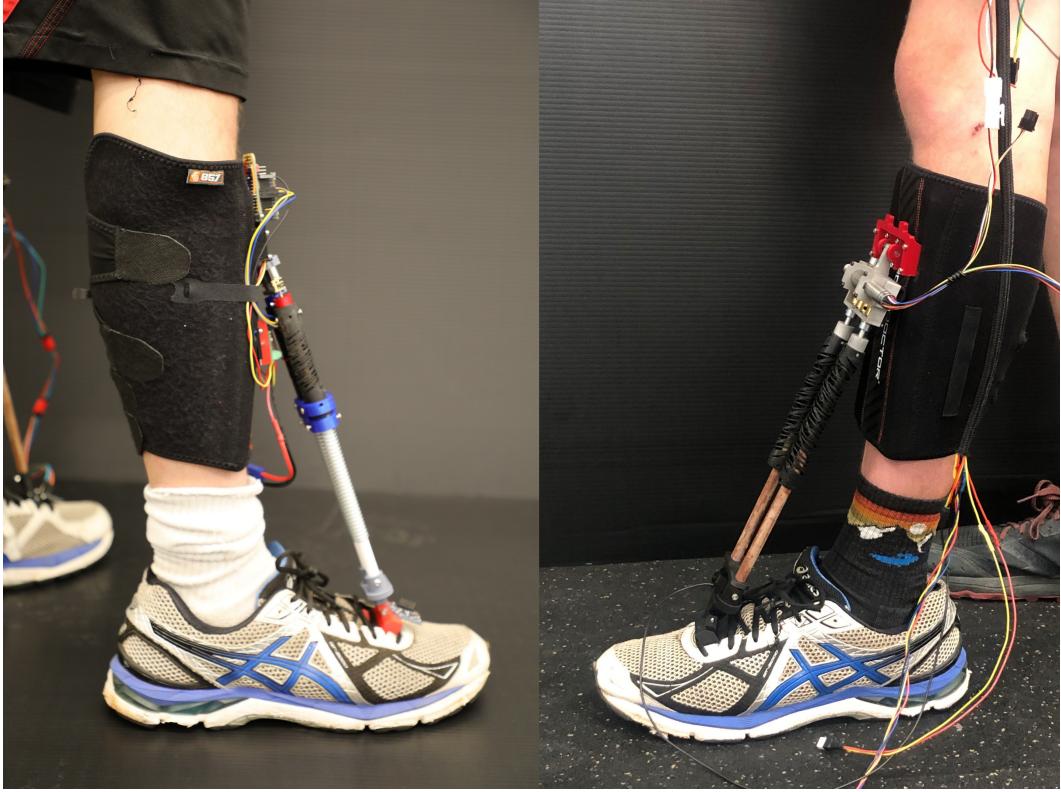
For user customization, the shin wrap's mounting height may be adjusted. The nominal location, shown in Figure 3.1, positions the linear actuation stage in an equilibrium position at stance. This position occurs when both the HSAs and compression springs are at their zero potential energy state. Users navigate to this state by adjusting the height of the shin wrap until the springs just begin to touch the base of the foot mount.

Hip Attachment

For the worm gearbox variant of the design, the electronics are located entirely at the hip apart from several key sensors (IMU, FSR, load cell) and the motors themselves. The hip pouch is split into a battery compartment housing a 5S lithium-polymer battery and an electronics compartment housing the control board. The control board includes a Teensy 4.1 with SD card logging, two electronic speed controllers (one for each leg), 2.4 GHz low-energy Bluetooth for wireless communication. Unlike the drone motor design, data is logged directly to the SD card and wirelss communication is used only for commands. Additionally, the control board manages exoskeletons on both legs simultaneously.

3.3   Actuation

The basic ankle exoskeleton design accommodates a wide range of actuation mechanisms, including passive and active designs. We tested the design with passive spring dynamics, drone motors, and a worm gearbox design. In each case, the design was optimized for weight, actuation surfaces, and durability. Figure 3.3 shows a comparison of these designs.
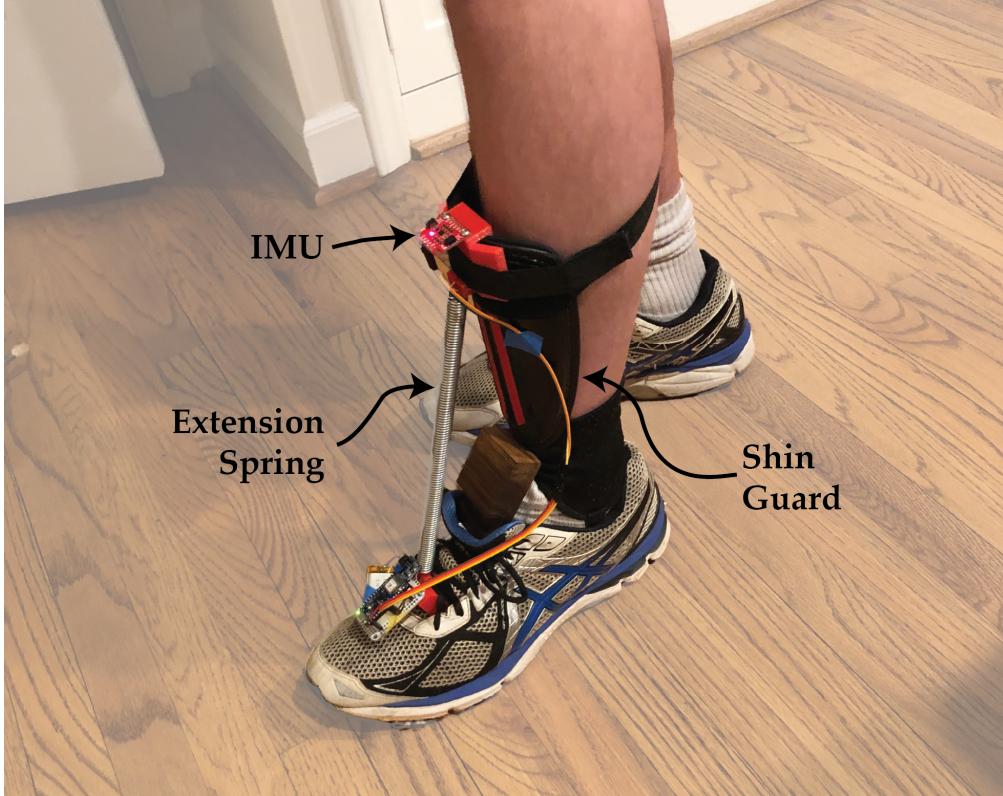
Figure 3.3: **Ankle Exoskeleton Design Comparison.** The drone motor design (left) and the worm gearbox design (right). Both designs share the majority of mounting hardware, but differ in their motor configuration. The worm gearbox design drives both HSAs with a single motor and has electronics located at the hip, while the drone motor design directly drives both HSAs with shin-mounted electronics.

Passive Dynamics Design

The first iteration of the ankle exoskeleton utilized the structure described above with a passive actuation mechanism replacing the HSAs. The goal of this design was to test the bodily attachment points under loads on the same order as the HSAs. We also used this design for a qualitative estimate of how low force HSA assistance could influence walking.

The design, pictured in Figure 3.4, replaced the HSA actuation stage with a single row of springs enclosing a telescoping tube. To test the compressive effects of HSAs, we assembled a passive dynamics actuation stage with two compression springs in series ($k_{eff} = 7.2$ N/mm). The springs were only attached at the shin, preventing them from applying forces in tension. This design was primarily targeted at testing possible push-off assistance.

To test assistance targeted at drop-foot, we used a single extension spring ($k = $
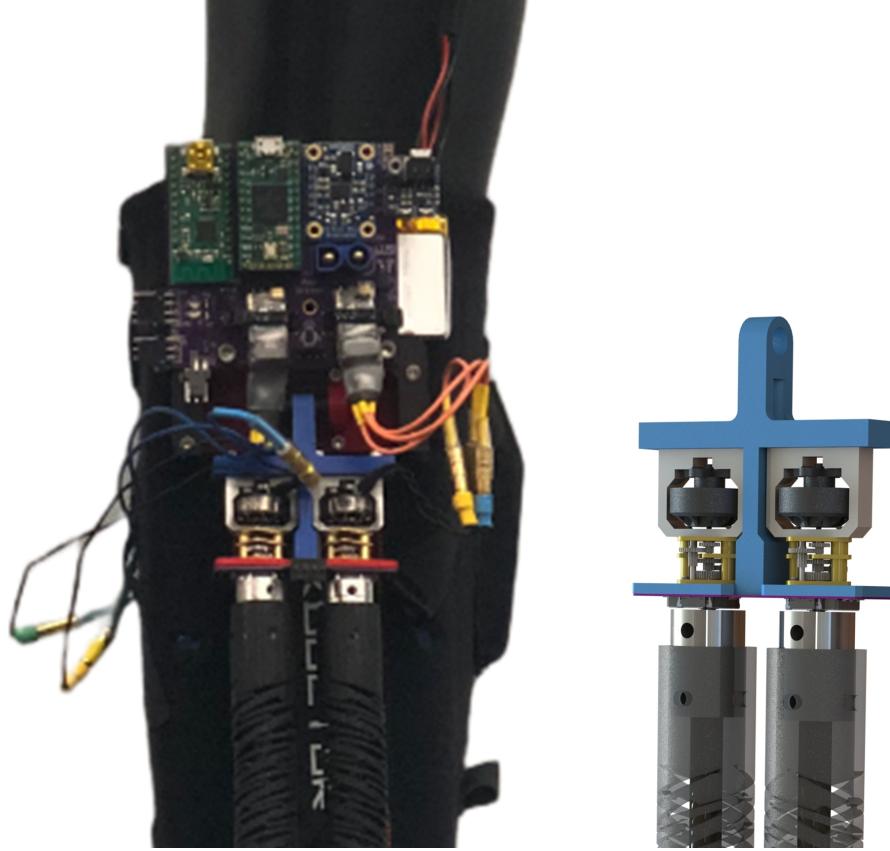
Figure 3.4: **Passive Extension-Spring Ankle Exoskeleton.** The earliest prototype ankle exoskeleton used a single extension spring or a pair of compression springs between the foot and shin mounts. This design was particularly useful for testing the exoskeleton's shin and shoe mounts, and for qualitatively predicting what an active HSA-based design might feel like.

0.415 N/mm) attached at both the shin and the foot with no telescoping tube. Shin height was adjusted so the spring did only pulled towards the end of the swing phase, protecting the user from drop-foot.

Drone Motor Design

The drone motor design directly drives each HSA with a rotary brushless motor (Flywoo 5150 Kv) coupled to a commerical gearbox (see Figure 3.5). The motor output shaft feeds through rotary potentiometers that measure the angle of rotation of each HSA for precise control and feedback. The entire spring-HSA system is mounted on a pair of telescoping tubes that guide the force onto the top of the foot and prevent buckling.

The specific motors (Flywoo 5150 Kv) were chosen to minimize weight. Driven at 11.1 V (a 3S battery), it has a no-load speed of 57,165 rpm. After gear reduction,
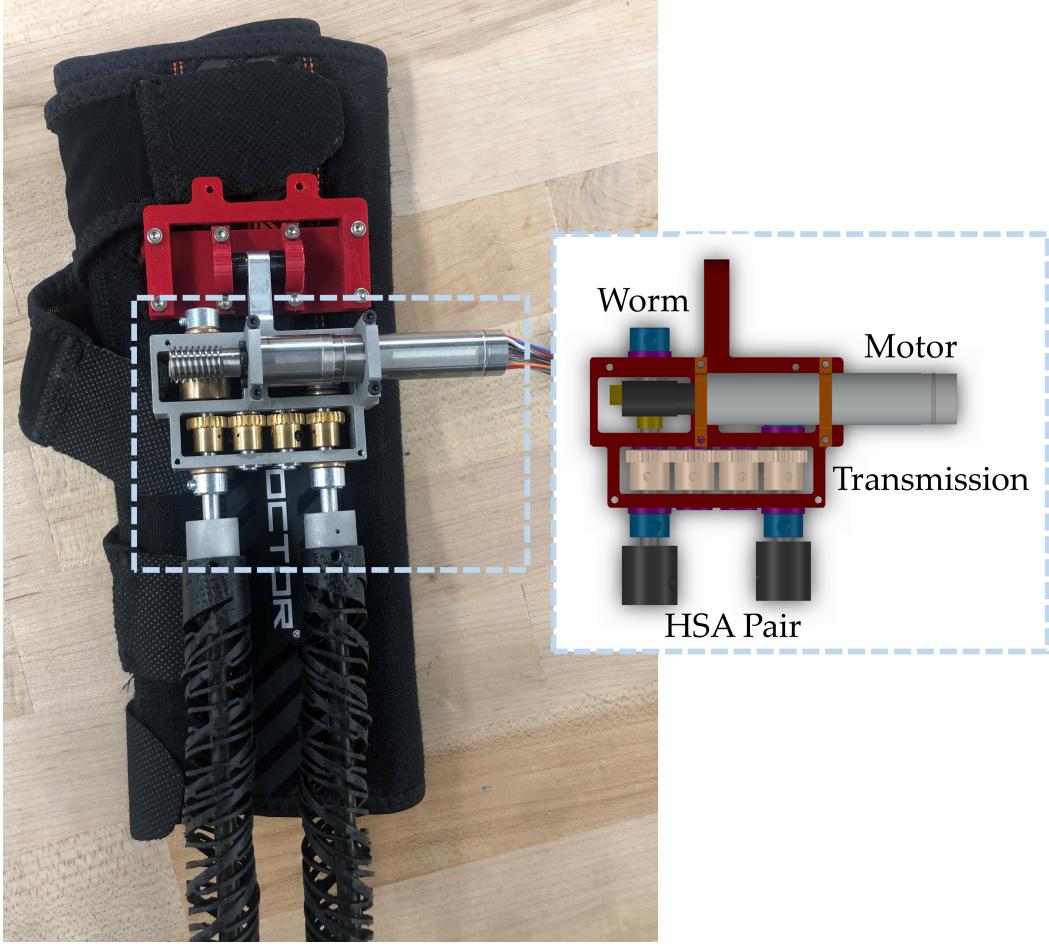
Figure 3.5: **Drone Motor Design Detail.** The drone motor design uses two compact brushless motors connected to a Pololu 100:1 gearbox to drive both HSAs. All electronics are mounted above on a single custom PCB.

this speed is reduced to about 570 rpm. The reported maximum power of the motor is 55 W, but our testing suggests the true power may be substantially lower. Further analysis of the motor and its limitations is given in Section 4.

Worm Gearbox Design

The brushless drone motor design is lightweight but incapable of applying enough torque to quickly move HSAs. Additionally, it fails to take advantage of the inherent symmetry of the task, requiring some low-level control to enforce zero-net-torque actuation. The drone motor design also suffers from frequent component breakage and backdrivablity, which compromises the inherent compliance of HSAs, increases wear, and complicates control.

To counter these issues, we designed a drive system specifically for HSAs. The gearing enforces that the two output shafts rotate in opposite directions with the same gear ratio (excluding backlash). It also uses a worm gear to prohibit backdrivability

Figure 3.6: **Worm Gearbox Design Detail.** Rather than actuate the two HSAs independently, the worm gearbox rotates both HSAs in opposite directions with the same motor. It also includes a worm that prevents backdrivability and a 50 W brushless motor.

and protect the actuating electronics. It's driven by a single powerful motor for each leg. The result is a compact, specialized drive system that produces linear actuation with minimal overhead. A diagram of the gearbox is shown in Figure 3.6.

Specifically, the gearbox is driven by a single brushless motor. The motor is a Maxon ECX SP 13L with a no-load speed of 65,800 rpm, a stall torque of 0.163 Nm, and a rated power of 50 W. A Maxon gearbox with ratio 5.3:1 is included on the output shaft of the motor. The output shaft is connected to a worm-worm gear configuration that adds a 20:1 reduction and directly turns one HSA. The other HSA is connected through four identical spur gears so it rotates in the opposite direction. This leaves the final gear ratio at 106:1. The output no-load speed is 621 rpm, and the output stall torque is 17.3 Nm. HSA loads are not expected to exceed 0.2 Nm. At

this load and with a 19 V supply (5S lithium-polymer battery), the expected motor speed is 485 rpm. This allows rapid rotation through the useful range of the auxetic trajectory, greatly improving the capabilities of the exoskeleton.

3.4   HSA Selection
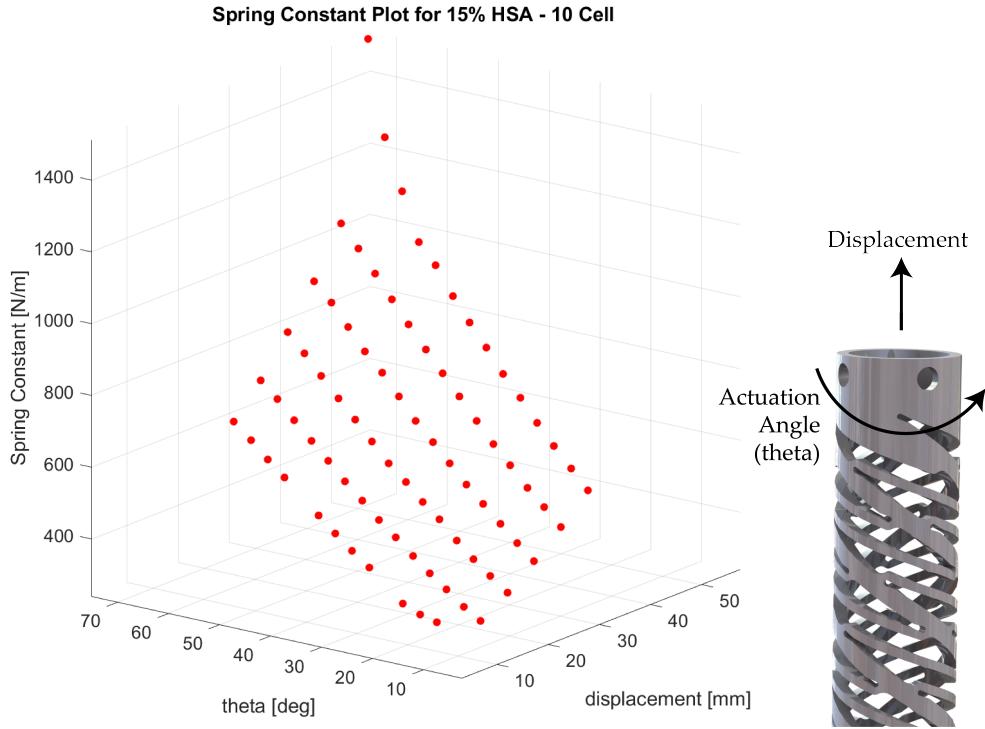
Minimum Viable Forces

To use HSAs in an exoskeleton they must be capable of applying enough force to provide noticeable assistance. As a conservative estimate, we assumed an inclined tube must be able to at least lift the weight of an adult foot (about 1 kg for a 60 kg person (Plagenhoef, Evans, and Abdelnour, 1983)). This conservative estimate puts the minimum viable force at 14 N, which HSAs are capable of applying at their peak. With our design, 14 N translates to about 1.2 Nm of torque applied to the ankle. For comparison, many large exoskeletons apply up to 300 N of force at their peak and maximum torques of around 50 Nm (Luke M Mooney, Rouse, and Hugh M Herr, 2014). With lower torques we can expect some metabolic cost reduction for carefully timed assistance, but it is unlikely we will be able to achieve the 20% or more energy cost reductions observed with high-torque exoskeletons.

HSA Parameters

HSA selection is inherently tied to control. As discussed in Section 1, historical developments with ankle exoskeletons relied on either (a) muscle-based control or (b) a tuned torque profile. Muscle-based control is particularly appealing for HSAs because of their variable stiffness property. If we designed an HSA to have parameters that were similar to a specific muscle along its auxetic trajectory, we could use the HSA to replace that muscle. While this is an appealing concept, this would require a more robust understanding of HSA parameter design than currently exists. Since the focus on this project is not on HSA development, we chose HSA parameters based on a tuned torque profile (parameterized) control framework.

For parameterized control, the spring constant of the HSAs can be effectively over-written with low stiffness springs in parallel and the HSAs behave like simple linear actuators. HSAs were designed and printed to exhibit a maximum length extension of 60 mm and a maximum length contraction of 10 mm. With these parameters, the HSA can extend to accommodate the large foot-to-shin distance during push-off and retract to prevent contact when the foot moves closer to the shin during swing. The true HSA displacement and spring constant values are shown in Figure 3.7.
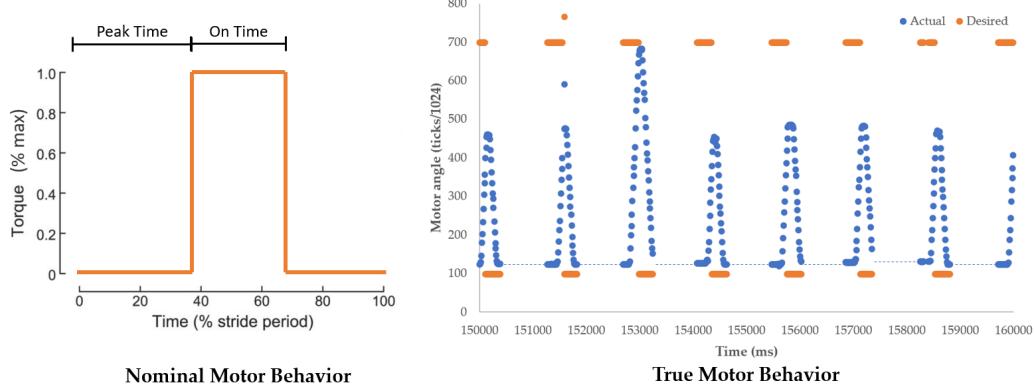
Figure 3.7: **HSA Characterization.** Our final HSA design was mechanically tested at the University of Washington. The independent variable (theta) represents the angle at which one end of the HSA was tested. Displacement is enforced by external clamps. The HSA is printed at 15% extension. Note that the spring constant increases with displacement from zero-force location and with angle of rotation.

3.5 Control Methodology

The exoskeleton's control targets assistance during the push-off phase of a user's gait. Our control algorithm is a parameterized curve that can be tuned for each individual user with preference-based learning or a parameter sweep. For the weaker, slower drone motor design we used a simple two-parameter bang-bang control. The discontinuous jumps are smoothed by slow motor dynamics. The worm gearbox design enables a much wider variety of complex control curves that include smoothing and more parameters.

Bang-Bang Control
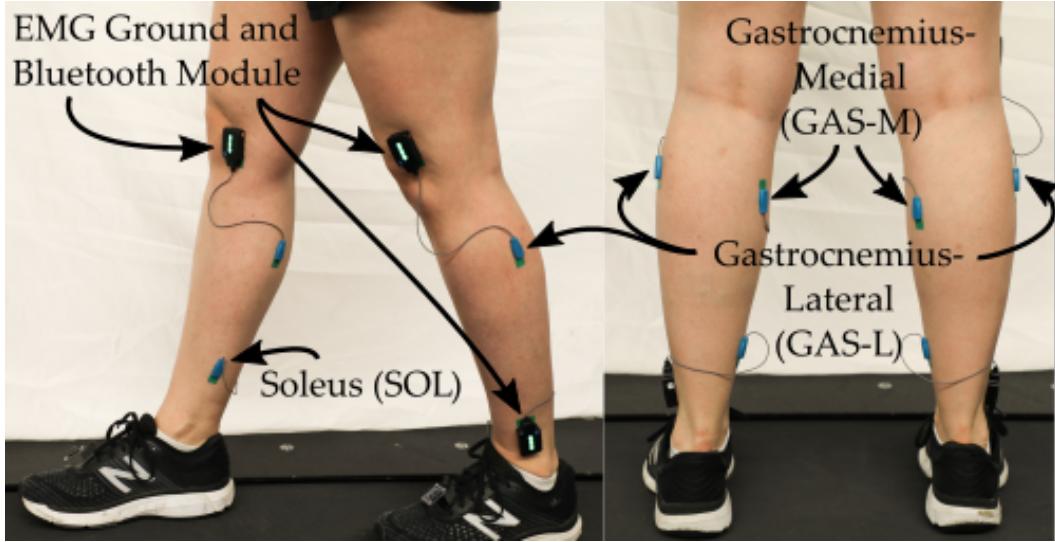
The basic control algorithm we use is bang-bang control (illustrated in Figure 3.8) because of the low force capabilities of HSA actuators. Assistance timing is determined by heel strike detection and a set of tunable time variables. The

Nominal Motor Behavior **True Motor Behavior**

Figure 3.8: **Control Paradigm**. We use a bang-bang control paradigm (left) to generate assistive torques. This style of control takes full advantage of the relatively weak HSA actuators. However, real angle data from our device (right) suggests that this idealized curve was not achieved in practice.

exoskeleton's heel-mounted FSR reliably detects heel strikes and records a rolling average of the user's step time. A tunable parameter s controls the time offset from heel strike at which actuation begins. This is stored as a percentage of total step time. Another parameter, Δs, determines the length of actuation in terms of the total step time. The HSAs are extended to their maximum safe length while actuated. After actuation, the HSAs are briefly retracted before returning to their zero-energy state.

Given the low torque capabilities and slow speed of the drone motor design, the nominal behavior of bang-bang control is practically impossible. The true behavior of the output is closer to a spike than a square wave (see Figure 3.8). Note that this is somewhat similar to the behavior of the biological power applied by the human during normal walking (Figure 3.2).

Figure 4.1: **EMG Sensor Placement.** Muscle activity was recorded from three muscles using electromyography (EMG): Gastrocnemius lateral head (GAS-L); Gastrocnemius medial head (GAS-M); and Soleus (SOL). The muscle activity was recorded using a Cosmed Trigno wireless EMG system with mini sensors. Each mini sensors has a EMG surface-mount sensor (the smaller blue sensor) and a larger module that houses an inertial measurement unit (IMU) sensor, a Bluetooth module, and records EMG ground.

Chapter 4

EXPERIMENTAL DEMONSTRATION

We performed a number of isolated metabolic cost and muscle activity tests with the ankle exoskeleton. Due to time constraints and mechanical failures, no extended experimental phase was carried out.

4.1 Electromyography with Drone Gearbox

We experimentally demonstrated the effect of our ankle exoskeleton for a single subject using electromygraphy (EMG) on specific muscles. Our subject was a healthy young adult female with no disabilities.

The subject was asked to walk on the treadmill continuously for three minutes at two different speeds (1.5 mph or 0.67 m/s, and 2.0 mph or 0.89 m/s) for the following three settings: wearing the exoskeleton with assistance provided, wearing the exoskeleton but no assistance provided, and without the exoskeleton. Before

testing, the subject was asked to adjust the shin wrap height for comfortable walking. The shin wrap was raised to disengage the springs before the no assistance trial. The subject used the same shoes between the three settings.

During all settings, in total of 18 minutes, electromyography (EMG) signals were recorded with the Trigno wireless biofeedback system (Delsys Inc.). Specifically, the activity of six muscles were recorded, including medial gastrocnemius(GAS-M), lateral gastrocnemius (GAS-L), and soleus (SOL) on each leg. Figure 4.1 shows the placement of EMG sensors.

Electromyography Results

The EMG results are shown in Figure 4.2. For the faster walking speed a large reduction in soleus muscle activity was observed during the push-off portion of the gait. A small increase in activity occurred during the swing portion. Additionally, the use of the exoskeleton when unpowered did not significantly affect the muscle activity.

These results were not uniform for both legs and across muscles. While the right soleus showed significant decline in muscle activity, it is difficult to compare the left soleus data across trials. An EMG sensor shift may have caused the drastic difference between the normal and unpowered walking for this reading. For the other two muscles measured, EMG reduction was significantly higher for the faster walking speeds.
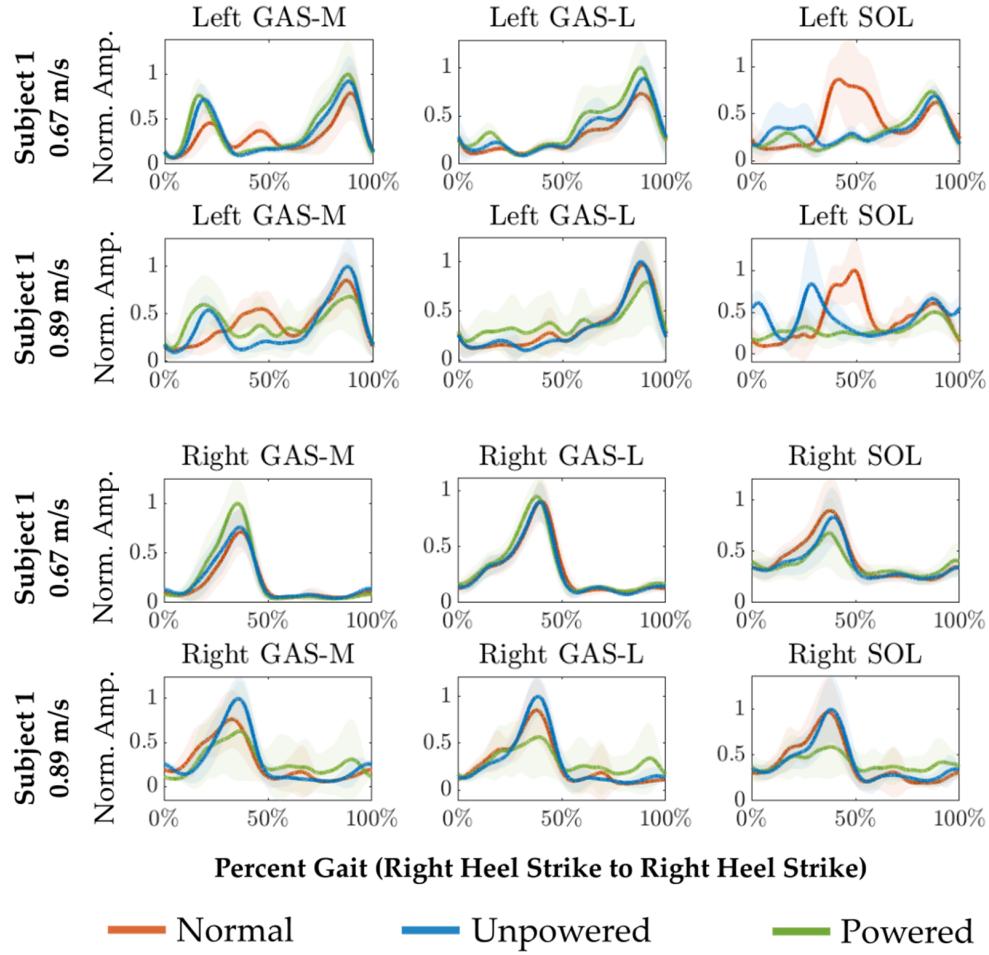
4.2   Metabolic Cost Tests with Drone Gearbox

We also evaluated the effects of our ankle exoskeleton on metabolic cost of transport through several walking trials with a single subject. Our subject was a healthy young adult male with no disabilities.

Experimental Procedure

Before each trial, the user self-tuned exoskeleton timing heuristically. A sweep of activation times *s* from 25% to 35% of the gait was performed at 1% increments. After the parameter sweep the user selected their preferred percentage and the powered exoskeleton setting proceeded.

During all settings (9 minutes total), metabolic cost of transport was recorded using a COSMED k4b2. Additionally, exoskeleton data was wirelessly recorded. This included compressive spring force, ankle angle, heel force, and motor commands.

Figure 4.2: **Experimental EMG Results.** The EMG results for subject 1 are presented for both a slower speed (1.5 mph or 0.67 m/s) and a faster speed (2 mph or 0.89 m/s). Both trials were conducted for 3 minutes on a treadmill. The EMG signals were then processed separately for each muscle, normalized to the maximum amplitude per muscle across both trials, and averaged across each complete gait cycle. The gait cycles begin with right heel strike.

Metabolic Cost Results

The metabolic cost results are shown in Figure 4.3. While they clearly show wearing the exoskeleton increases the metabolic cost of transport, they do not demonstrate any benefit to powered exoskeleton assistance. Assisted and unassisted walking had nearly identical metabolic costs that were just above the metabolic cost of walking without wearing a powered or unpowered exoskeleton.
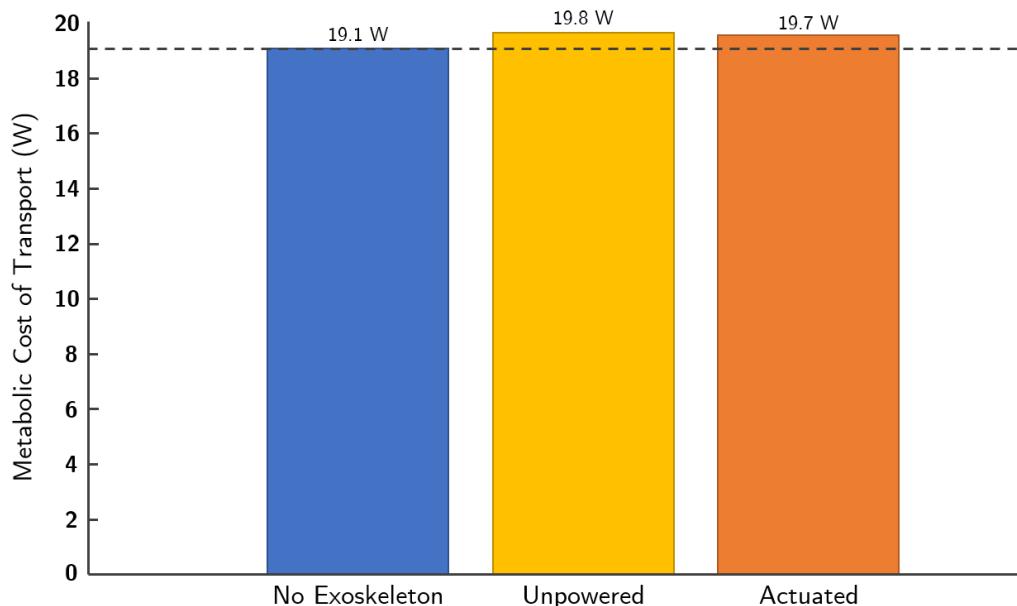
Figure 4.3: **Metabolic Cost of Transport Results.** Metabolic cost data for our subject does not show any effect of exoskeleton assistance. Compared to the no assistance setting, applying assistance at 31% of the gait had almost no effect on metabolic cost of transport. Wearing the exoskeleton did increase metabolic cost, but only by a relatively small amount.

Chapter 5

DISCUSSION

Although our quantitative experimental data is not conclusive about the beneficial effects of our exoskeleton, it does suggest significant possibility for assistance. Aside from EMG and metabolic cost data, we collected a range of sensor information that can help analyze how the exoskeleton operated. This section discusses the limitations of our exoskeleton and proposes several directions for further research.

5.1 Metabolics and EMG Results

The metabolics and EMG results are somewhat inconsistent. While EMG suggests the exoskeleton significantly lowered the activity of a particular muscle, metabolics data shows the exoskeleton had essentially no effect on total caloric expenditure. These results are not inherently contradictory: although the activity of at least one muscle was reduced, activity may have increased in other muscles due to our assistance. Further, the two trials were run with different subjects.

Together, these quantitative results are somewhat positive. One major concern for the weakly-actuated HSA-based ankle exoskeleton is not enough force to provide meaningful assistance. Muscle activity reduction measured by EMG suggests that the exoskeleton can in fact affect the body, an observation not inherently clear from the metabolics data. This directs attention towards control and helps justify the use of HSAs in future exoskeleton work.

5.2 Analysis of Limitations

Three key limitations stand out as major issues with the exoskeleton that contributed to its poor performance. First, the inherently fragile and weak HSA actuators significantly limit the total force that can be applied. Second, hardware breakage and low-torque motors reduce the range of possible control algorithms and requires slow adaptation to the human body. Third, the control itself is very simple and contains only a limited amount of tunable parameters. These limitations are especially clear from sensor data taken during the trials.

Sensor Data During Metabolic Cost Trials

Exoskeleton sensors provide some indication of how the exoskeleton operated. Figure 3.8 illustrates the averaged actuation profile of the ankle exoskeleton over the course of the gait. Note that even at peak actuation, the compressive (pushing) force of the ankle exoskeleton increases, but remains relatively small. The large standard deviation is due in part to a steady decline in compressive force over the course of the trial, likely caused by hardware issues. Ankle angle data also follows this trend, with angles converging to the unpowered ankle angle as the trial continued.

Also of note is the large difference between the commanded motor angle and the true motor angle, shown in Figure 3.8. There is a 50 ms delay between motor command and movement. Additionally, while the motors are able to stop quickly they take nearly 70 ms to reach their maximum angle. This suggests the motors do not have enough power (torque and speed) to reasonably match our desired control curve.

Hardware Failure

Hardware issues with the drone gearbox were also an issue. During metabolic cost trials, the gearbox needed to be replaced every three minutes due to a stripped gear. The major cause of this issue was high backdriven loads: when the HSA pushes against the foot, the load on the motor significantly increases. Backdrivability reflects how the range of limitations of the ankle exoskeleton are confounded: the HSAs are inherently weak, but so is the hardware that is driving them. Trajectory tracking is especially difficult when control itself is backdrivable. For this reason, the muscle activity reductions observed in EMG data are especially hopeful because they suggest that even the drone exoskeleton can overcome these limitations and affect the body.

5.3   Future Directions

The range of future directions for this project is huge. The first step should be testing our existing control with the more powerful worm gearbox. This design eliminates backdrivability, timing issues, and hardware failure, allowing full use of the HSA. It allows for a renewed focus on control and state estimation far beyond simple bang-bang control with heel-strike state estimation. Much faster control algorithms can be implemented and tuned using this new hardware. To be effective, these control algorithms must be paired with accurate state estimation of where the user is in the gait and where the user intends to move.

Beyond immediate term testing, HSA-based ankle exoskeletons have enormous

potential for a broad range of applications. Once hardware is stable, HSAs could be designed to fit the user or to replace or train a muscle. HSA-based exoskeletons have inherent compliance that is difficult to take advantage of without co-design of control with HSA parameters. The benefits of this co-design could include devices that assist with injury recovery or allow their user to carry heavier loads or help their user train for an event.

Although this HSA-based ankle exoskeleton has not yet shown metabolic cost reduction, it is a strong step towards a future with more compliant, customized, and lightweight exoskeletons that could assist with a broad range of tasks.

Chapter 6

CONCLUSIONS

This work presents two main contributions: 1) the novel design of an ankle exoskeleton that utilizes Handed Shearing Auxetics (HSAs) and minimal user-specific hardware; 2) experimental demonstration of the device across a single subject.

The novelty of the design appears in two places. First, it is the only (to the best of our knowledge) design that mounts to the anterior portion of the lower leg. This leads to less protrusion from the body, allowing the user to cross their legs freely. Second, the proposed design leverages HSAs, which provide a lightweight and flexible mechanism for translating rotational torques into linear translations. The experimental results illustrate the difficulty of working with soft and lightweight materials, but we are hopeful that further control refinement can lead to substantive energy cost reduction during walking.

The preliminary nature of this work leaves many next steps for the HSA ankle exoskeleton. These include expanding the experimental protocol to include metabolic cost measurements with more subjects, implementing a systematic method (such as preference-based learning) of tuning the user-specific control parameters for each subject, and evaluating the effect of actuation timing on varying walking speeds.

Overall, this work demonstrates a novel ankle exoskeleton design capable of moving the field towards more lightweight and flexible devices, a promising advancement for the field of wearable devices.

BIBLIOGRAPHY

Antonellis, Prokopios et al. (Mar. 2022). "Metabolically efficient walking assistance using optimized timed forces at the waist". In: *Science Robotics* 7.64. DOI: 10.1126/scirobotics.abh1925. URL: https://doi.org/10.1126/scirobotics.abh1925.

Collins, Steven H., M. Bruce Wiggin, and Gregory S. Sawicki (Apr. 2015). "Reducing the energy cost of human walking using an unpowered exoskeleton". In: *Nature* 522.7555, pp. 212–215.

Ferris, Daniel P. et al. (2006). "An improved powered ankle–foot orthosis using proportional myoelectric control". In: *Gait and Posture* 23.4, pp. 425–428. ISSN: 0966-6362. DOI: https://doi.org/10.1016/j.gaitpost.2005.05.004. URL: https://www.sciencedirect.com/science/article/pii/S0966636205001049.

Galle, S. et al. (July 2013). "Adaptation to walking with an exoskeleton that assists ankle extension". In: *Gait and Posture* 38.3, pp. 495–499. DOI: 10.1016/j.gaitpost.2013.01.029. URL: https://doi.org/10.1016/j.gaitpost.2013.01.029.

Galle, Samuel et al. (Apr. 2017). "Reducing the metabolic cost of walking with an ankle exoskeleton: interaction between actuation timing and power". In: *Journal of NeuroEngineering and Rehabilitation* 14.1. DOI: 10.1186/s12984-017-0235-0. URL: https://doi.org/10.1186/s12984-017-0235-0.

Good, Ian et al. (2021). "Expanding the Design Space for Electrically-Driven Soft Robots through Handed Shearing Auxetics". In: *arXiv preprint arXiv:2110.00669*.

Johansson, Melker Staffan et al. (Oct. 2019). "Time spent cycling, walking, running, standing and sedentary: a cross-sectional analysis of accelerometer-data from 1670 adults in the Copenhagen City Heart Study". In: *BMC Public Health* 19.1. DOI: 10.1186/s12889-019-7679-z. URL: https://doi.org/10.1186/s12889-019-7679-z.

Kao, Pei-Chun, Cara L. Lewis, and Daniel P. Ferris (Jan. 2010). "Invariant ankle moment patterns when walking with and without a robotic ankle exoskeleton". In: *Journal of Biomechanics* 43.2, pp. 203–209. DOI: 10.1016/j.jbiomech.2009.09.030. URL: https://doi.org/10.1016/j.jbiomech.2009.09.030.

Lipton, Jeffrey Ian et al. (2018). "Handedness in shearing auxetics creates rigid and compliant structures". In: *Science* 360.6389, pp. 632–635.

Mooney, Luke M, Elliott J Rouse, and Hugh M Herr (2014). "Autonomous exoskeleton reduces metabolic cost of human walking during load carriage". In: *Journal of NeuroEngineering and Rehabilitation* 11.1, p. 80.

Mooney, Luke M. and Hugh M. Herr (Jan. 2016). "Biomechanical walking mechanisms underlying the metabolic reduction caused by an autonomous exoskeleton". In: *Journal of NeuroEngineering and Rehabilitation* 13.1. DOI: `10.1186/s12984-016-0111-3`. URL: `https://doi.org/10.1186/s12984-016-0111-3`.

Plagenhoef, Stanley, F. Gaynor Evans, and Thomas Abdelnour (June 1983). "Anatomical Data for Analyzing Human Motion". In: *Research Quarterly for Exercise and Sport* 54.2, pp. 169–178. DOI: `10.1080/02701367.1983.10605290`. URL: `https://doi.org/10.1080/02701367.1983.10605290`.

Slade, Patrick et al. (Oct. 2022). "Personalizing exoskeleton assistance while walking in the real world". In: *Nature* 610.7931, pp. 277–282. DOI: `10.1038/s41586-022-05191-1`. URL: `https://doi.org/10.1038/s41586-022-05191-1`.

Takahashi, Kota Z, Michael D Lewek, and Gregory S Sawicki (2015). "A neuromechanics-based powered ankle exoskeleton to assist walking post-stroke: a feasibility study". In: *Journal of neuroengineering and rehabilitation* 12.1, pp. 1–13.

Truby, Ryan L, Lillian Chin, and Daniela Rus (2021). "A recipe for electrically-driven soft robots via 3d printed handed shearing auxetics". In: *IEEE Robotics and Automation Letters* 6.2, pp. 795–802.

Zelik, Karl E. and Peter G. Adamczyk (Dec. 2016). "A unified perspective on ankle push-off in human walking". In: *Journal of Experimental Biology* 219.23, pp. 3676–3683. DOI: `10.1242/jeb.140376`. URL: `https://doi.org/10.1242/jeb.140376`.

Zhang, Juanjuan et al. (2017). "Human-in-the-loop optimization of exoskeleton assistance during walking". In: *Science* 356.6344, pp. 1280–1284.